European Journal of Pharmaceutics and Biopharmaceutics 202 (2024) 114410

Contents lists available at ScienceDirect

European Journal of Pharmaceutics and Biopharmaceutics

journal homepage: www.elsevier.com/locate/ejpb

Paradoxical cell targeting of calreticulin-empowered, protein-only nanoparticles

Eloi Parladé [a,b,1,*], Annabel García-Leon [b,c,d,1], Eric Voltà-Durán [a,b,e], Ugutz Unzueta [b,c,d,e], Ramon Mangues [b,c,d], Isolda Casanova [b,c,d,*], Antonio Villaverde [a,b,e,*], Esther Vázquez [a,b,e]

[a] Institut de Biotecnologia i de Biomedicina, Universitat Autònoma de Barcelona, Plaça Cívica s/n, Bellaterra, 08193 Barcelona, Spain
[b] CIBER de Bioingeniería, Biomateriales y Nanomedicina (CIBER-BBN), C/ Monforte de Lemos 3-5, 28029 Madrid, Spain
[c] Institut de Recerca Sant Pau (IR SANT PAU), Sant Quintí 77-79, 08041 Barcelona, Spain
[d] Josep Carreras Leukaemia Research Institute (IJC), Carretera de Can Ruti, Badalona, 08916, Barcelona, Spain
[e] Departament de Genètica i de Microbiologia, Universitat Autònoma de Barcelona, Plaça Cívica s/n, Bellaterra, 08193 Barcelona, Spain

ARTICLE INFO

Keywords:
Recombinant proteins
Protein materials
Nanoparticles
Drug delivery
Cell targeting

ABSTRACT

Surface-exposed calreticulin (CRT) serves as a crucial cell damage-associated molecular pattern for immunogenic apoptosis, by generating an "eat me" signal to macrophages. Aiming at precision immunotherapies we intended to artificially label tumoral cells in vivo with a recombinant CRT, in a targeted way. For that, we have constructed a CRT fusion protein intended to surface attach CXCR4^{+} cancer cells, to stimulate their immunological destruction. As a targeting ligand of the CRT construct and to drive its specific cell adhesion, we used the peptide V1, a derivative of the vMIP-II cytokine and an antagonist of CXCR4. The modular protein tends to self-assemble as regular 16 nm nanoparticles, assisted by ionic Zn. Through both in vivo and in vitro experiments, we have determined that CRT itself confers cell targeting capabilities to the construct overcoming those of V1, that are only moderate. In particular, CRT binds HeLa cells in absence of further internalization, by a route fully independent of CXCR4. Furthermore, by cytometry in THP-1 cells, we observed that the binding of the protein is preferential for dead cells over live cells, a fact that cannot be associated to a mere artefactual adsorption. These data are discussed in the context of the oligomerizing properties of CRT and the potential clinical applicability of proteins and protein materials functionalized with this novel cell surface ligand.

1. Introduction

Despite the development of many innovative approaches, the therapy of cancer is still based on the systemic administration of cytotoxic drugs [1,2]. Being untargeted, chemotherapies present systemic toxicity and severe off-target effects [1], in addition to drug resistance [3]' these issues pushing to explore alternative therapeutic approaches. In this regard, the increasingly recognized contribution of the immune system to the natural control of cancer [4–7] opens a set of novel therapeutic possibilities [8–11]. Among them, the stimulation of the adaptive immune system and the inhibition of T cell checkpoints aim at overcoming aberrant cell proliferation. In this sense, phagocytic cells such as macrophages are a key cell type for destruction of tumor cells in different types of cancer [12,13]. One of the dominant pro-phagocytic signals is the protein calreticulin (CRT) [14–16], usually found in the endoplasmic reticulum (ER) lumen serving as a chaperone, but occasionally translocated to the cell surface and acting as a "eat me" signal in contrast to the "don't eat me" CD47 signal [17]. Surface-exposed CRT (ectoCRT) is translocated from the ER in stressful situations, and it serves as a crucial damage-associated molecular pattern for immunogenic apoptosis [18]. The presented ectoCRT is to be recognized by the low-density lipoprotein receptor-related protein 1 (LRP1 or CD91) occurring in macrophages and dendritic cells, thus activating the cellular machinery responsible for apoptotic cell phagocytosis [19]. Interestingly, this pro-phagocytotic signaling caused by the recognition of ectoCRT can be counterbalanced by CD47. Also known as the "don't eat me" signal [20]

* Corresponding authors at: Institut de Biotecnologia i de Biomedicina, Universitat Autònoma de Barcelona, Plaça Cívica s/n, Bellaterra, 08193 Barcelona, Spain (E. Parlade, A. Villaverde) and CIBER de Bioingeniería, Biomateriales y Nanomedicina (CIBER-BBN), C/ Monforte de Lemos 3-5, 28029 Madrid, Spain (I. Casanova).
E-mail addresses: eloi.parlade@uab.cat (E. Parladé), icasanova@santpau.cat (I. Casanova), antonio.villaverde@uab.cat (A. Villaverde).
[1] These authors contributed equally to the work.

https://doi.org/10.1016/j.ejpb.2024.114410
Received 26 April 2024; Received in revised form 4 July 2024; Accepted 10 July 2024
Available online 14 July 2024

this immunoglobulin is overexpressed on the surface of immune-evading cancer cells of several cancer types including AML, non-Hodgkin lymphoma, and bladder cancer [21]. The antagonization or blockade of CD47 has been the main approach in recent attempts to stimulate innate immune response against cancer cells [22]. Unfortunately, antagonistic peptides are rapidly removed from the bloodstream via renal filtration due to their small size [23], and CD47-blocking antibodies are in general unable to trigger macrophage phagocytosis by themselves, requiring combined therapy with other antibodies that opsonize for destruction [24].

In previous research, we have identified and characterized several ligands of the cell-surface tumoral marker CXCR4 [25,26], overexpressed in more than 20 human neoplasias [27–31], and successfully displayed them in self-assembling protein nanoparticles for cell targeted cancer therapies [32,33]. These CXCR4-targeted materials have been carriers for low molecular weight drugs [34–36] and cytotoxic [32,37,38], pro-apoptotic [39] or pyroptotic proteins [40,41]. In the present study, we have initially tested the ability of the peptide V1, a CXCR4 ligand derived from vMIP-II (N-terminal residues 1–21) with poor internalization activities, to promote binding of CRT to the $CXCR4^+$ cancer cell surface for the targeted activation of phagocytic cells. However, by taking this approach, we have identified unexpected targeting activities of CRT itself, as a functional component of protein nanoparticles, that impose over those conferred by V1. The mechanics of CRT-mediated cell targeting is discussed in the context of its potential clinical applicability as a novel cell surface ligand in oncology.

2. Experimental section

2.1. Protein production, purification, and characterization

Proteins were designed in-house, and the encoding codon-optimized genes were provided by GeneArt (Thermo Fisher) already subcloned into pET22b plasmids (Novagen). Then, protein-encoding plasmids were transformed into *Escherichia coli* BL21 (DE3; Novagen) and production carried out overnight (O/N) at 20 °C and 250 rpm agitation in Lysogeny Broth (LB) medium upon induction with 0.1 mM isopropyl-β-D-1-tio-galactopyranoside (IPTG). Cells were then harvested by centrifugation (15 min at 5,000 g) and resuspended in wash buffer (20 mM Tris-HCl, 500 mM NaCl, 10 mM Imidazole, pH 8) in presence of protease inhibitors (cOmplete™ EDTA-Free, Roche). Cells were then disrupted in an EmulsiFlex-C5 system (Avestin) by 4 rounds at 8,000 psi. The soluble fraction of the cell lysate, containing the proteins, was separated by centrifugation (45 min at 15,000 g), filtered through 0.45 and 0.22 μm pore filters, and then charged into a HisTrap HP column (Cytiva) for purification by immobilized metal affinity chromatography (IMAC) in an ÄKTA pure system (Cytiva). Proteins of interest were eluted using a lineal gradient of elution buffer (20 mM Tris, 500 mM NaCl, 500 mM Imidazole, pH 8) and dialyzed against a sodium carbonate salt buffer (166 mM $NaCO_3H$, 333 mM NaCl pH 8). Protein purity was assessed via sodium dodecyl-sulfate polyacrylamide gel electrophoresis (12 % TGX Stain-Free™ FastCast™ Acrylamide Kit, BioRad), followed by western-blot immunodetection utilizing an anti-His monoclonal antibody (Santa Cruz Biotechnology). Finally, protein integrity was verified through matrix-assisted laser desorption ionization time-of-flight (MALDI-TOF) mass spectrometry (Supplementary Fig. 1A). The design and production of GPF-H6 and T22-GFP-H6 proteins is described elsewhere [25].

2.2. Nanoparticle assembly and morphometric characterization

The protein concentration was adjusted to 3 mg/ml in a sodium carbonate salt buffer (166 mM $NaCO_3H$, 333 mM NaCl, pH 8) before initiating nanoparticle assembly, with the addition of 0.6 mM $ZnCl_2$. Disassembly of the nanoparticles was achieved using 1.2 mM ethylenediamine tetraacetic acid (EDTA). Volume size distribution (expressed in nm) of protein constructs was determined in a Zetasizer Pro particle analyzer (Malvern Instruments). Size was measured by Dynamic Light Scattering (DLS) at 633 nm. Green fluorescence emission (510–580 nm) was measured in Qubit™ 4 Fluorometer (Invitrogen) after excitation with blue LED light (430–495 nm). Fluorescence was measured at equimolar protein concentrations (300 nM).

2.3. Animal maintenance

Four-week-old female Swiss Nude mice were obtained from Charles River Laboratories. Mice were maintained in specific pathogen-free (SPF) conditions with sterile food and water *ad libitum*. Experimental procedures were reviewed and approved by the Institutional Animal Care and Use Committee of the Sant Pau Research Institute and authorized by the Animal Experimental Committee of the local government authority (Generalitat de Catalunya, authorization No. 10108) in accordance with the Spanish Law (RD 53/2013) and European Directive 2010/63/EU. Procedures were performed at the Animal Experimentation Service, ISO 9001:2015 certified. In addition, the investigation adheres to the Guide for the Care and Use of Laboratory Animals published by the US National Institutes of Health (NIH Publication No. 85–23, revised 1985) and the ARRIVE guidelines (Animal Research: Reporting of In Vivo Experiments), and upholds the principles of the 3Rs in laboratory animal research, thereby utilizing the minimum number of animals necessary to achieve statistical significance.

2.4. In vivo biodistribution of V1-GFP-pcCRT-H6 in THP-1 subcutaneous (SC) mouse model

The nanoparticle biodistribution was evaluated in a well-established SC mouse model of Acute Myeloid Leukemia, commonly used for studies involving CXCR4 interactions [42]. Firstly, 10 million THP-1 cells were injected subcutaneously into the dorsal region of a Swiss Nude mice. Tumor growth was monitored twice a week with caliper measurements (tumor volume = $width^2$ x length/2). Animal weight was recorded throughout the experimental period. When tumors reached a volume between 300 and 400 mm^3, mice received a single intravenous dose of carbonate salt buffer (166 mM $NaCO_3H$, 333 mM NaCl pH 8), 200 mg GFP-H6 or 200 mg V1-GFP-pcCRT-H6. Animals were euthanized at 1 (n = 2), 5 (n = 2), and 24 h (n = 1) post-injection. Fluorescence intensity, expressed as average radiant efficiency, was measured *ex vivo* in each tissue, using the IVIS Spectrum 200 Imaging System (PerkinElmer), to quantify the accumulation of GFP-H6 or V1-GFP-pcCRT-H6, detected by the fluorescence emission of the GFP domain. The FLI of experimental mice was determined by subtracting the autofluorescence observed in control mice injected with buffer.

2.5. Cell culture

To investigate the specificity of our ligand V1, we employed cancer cell lines overexpressing CXCR4, namely human cervix-derived HeLa cells and acute myeloid leukemia-derived THP-1 cells. Overexpression of CXCR4 in such cell lines was confirmed and described elsewhere [38]. HeLa cells (ATCC, CCL-2) were nurtured in MEM alpha medium (Gibco) supplemented with 10 % Fetal Bovine Serum (FBS, Gibco) within a 5 % CO_2 humidified atmosphere at 37 °C. Concurrently, THP-1 cells (Leibniz Institute DSMZ, ACC16) were cultured in RPMI-1640 medium complemented with 10 % FBS, 10 mM L-glutamine, 100 U/mL penicillin, and 10 mg/ml streptomycin, maintained at 37 °C in a 5 % CO_2 humid environment.

2.6. Confocal microscopy

In confocal microscopy experiments, HeLa cells were cultured on MatTek plates (MatTek Corporation, Ashland, MA, USA) at a density of 200,000 cells per plate over a 24-hour period. Subsequently, MEM Alpha

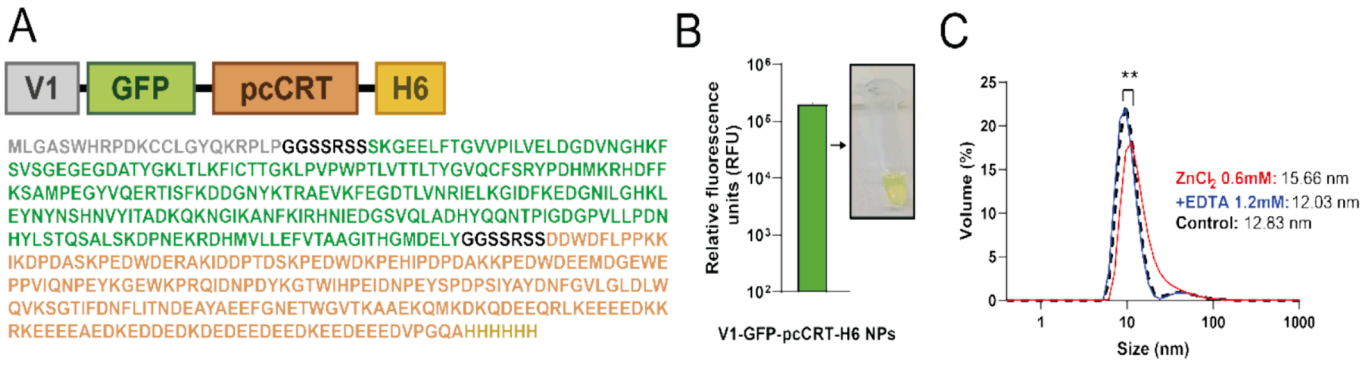

Fig. 1. Description and characterization of V1-GFP-pcCRT-H6. A. Modular organization and amino acid sequence of V1-GFP-pcCRT-H6. B. Green fluorescence emission (510–580 nm) of the assembled protein upon excitation with blue LED light (430–495 nm). In the inset, straightforward fluorescent emission of the protein solution. C. Volume-size distribution and mean size determination via DLS of the recombinant V1-GFP-pcCRT-H6 in unassembled (black), Zn-assembled (red) and EDTA-disassembled (blue) forms. Differences between the peak size values of assembled and disassembled samples are statistically significant (**; $p < 0.01$).

was replaced with OptiProTM serum-free medium (Gibco), and the cells were exposed to the proteins of interest for 2 to 24 h, depending on the assay. Following exposure to the protein materials, cell nuclei were labeled with 5 μg/ml Hoechst 33,342 (ThermoFisher), and plasma membranes were stained with 2.5 μg/ml CellMask™ Deep Red (ThermoFisher) for 10 min at room temperature. After washing with DPBS (Sigma-Aldrich), visualization was conducted in MEM alpha medium using an inverted TCS SP5 Leica Spectral confocal microscope (Leica Microsystems) equipped with a 63× (1.4NA) oil immersion objective lens. Excitation was reached using a 405 nm blue diode laser for Hoescht, a 488 nm diode laser for GFP-containing constructs, and a 633 nm diode laser for CellMask™. Emission detection bandwidths were meticulously optimized to avoid cross-talk. The confocal pinhole was set to 95.4 μm and fluorescence detection voltages were tailored for each photomultiplier tube (PMT) sensor. The PMT1 sensor, responsible for Hoechst detection, operated at a fixed gain voltage of 790 V. For CellMask™ detection (PMT4) and GFP fluorescence detection (PMT2), voltages ranged from 797 V to 859 V and from 710 to 890 V, respectively. Higher voltages were used specifically to explore potential traces in samples lacking green fluorescence. Image processing was carried out using Leica Application Suite X software version 3.5.7.

2.7. Flow cytometry

Flow cytometry protein binding studies were performed with THP-1 cells, known for their suspension growth. This choice was guided by the advantage that trypsinization, which is not required for THP-1 cells, could otherwise remove the bound protein in HeLa cells. Additionally, the FSC/SSC profile of HeLa cells in cytometry does not resolve alive and dead populations as clearly as observed in THP-1 cells, based on our previous studies. Specifically, analyses were conducted using a CytoFLEX Flow Cytometer (Beckman Coulter) equipped with a 488 nm blue diode laser for excitation. 10,000 events were registered for each sample replicate. Green fluorescence emission was detected via the FITC channel, equipped with a 525/40 band pass filter. For fluorescence determination, the primary focus was on the live cell population designated as P1. This population was carefully gated based on forward scatter (FSC-A) and side scatter (SSC-A) parameters, ensuring the selection of viable cells (Supplementary Fig. 1B). During gate definition, a secondary population (P2) was explored within the realm of dead cells and debris. Despite its origin in non-viable cells, this population exhibited significantly enhanced binding of the fluorescent protein. To validate that Population P2 was composed of dead cells, we performed propidium iodide (PI) staining. PI, a nucleic acid stain that penetrates only dead cells with compromised membranes, was used at a final concentration of 2 μg/mL in phosphate-buffered saline (pH 7.4). After incubation, cells were analyzed by flow cytometry. Dead cells exhibited increased red fluorescence in the PE-A channel. As expected, Population P2 showed a significant increase in red fluorescence, confirming it consisted predominantly of dead cells (Supplementary Fig. 2). Raw data processing was conducted in the Cytexpert software version 2.4.

2.8. Statistical analysis and data visualization

All graphs and statistical analyses were performed in GraphPad Prism 8.0.2. Quantitative data were expressed as mean ($\bar{x}$) ± Standard

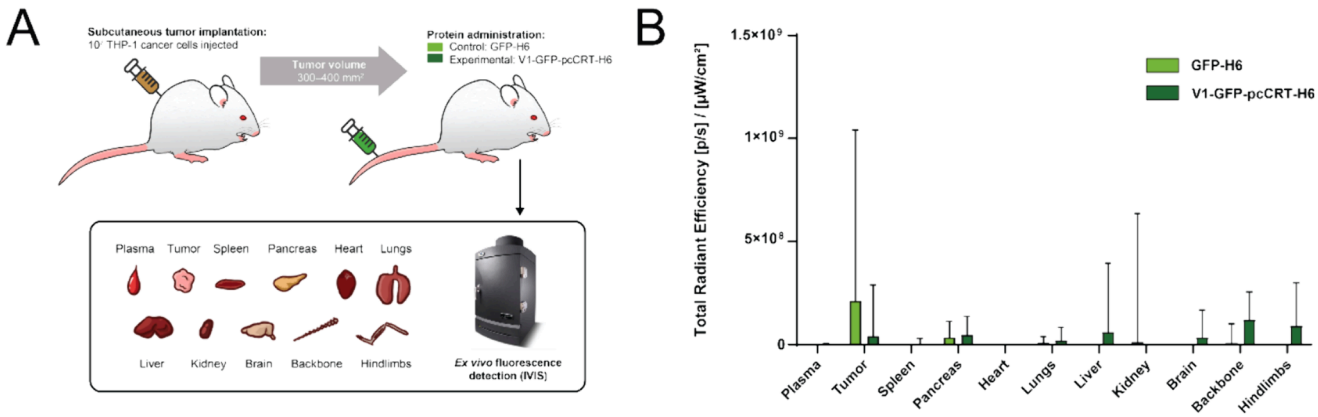

Fig. 2. A: Scheme of the in vivo biodistribution assay of the recombinant GFP-H6 and V1-GFP-pcCRT-H6 in the $CXCR4^{+}$ SC THP-1 mouse model. B: Biodistribution after injection of the protein in plasma, tumor, and major organs. Data presented is the average of all time points (1 h, 5 h, and 24 h). Basal levels of autofluorescence of each organ, as measured after injection of buffer solution, were subtracted to the experimental values.

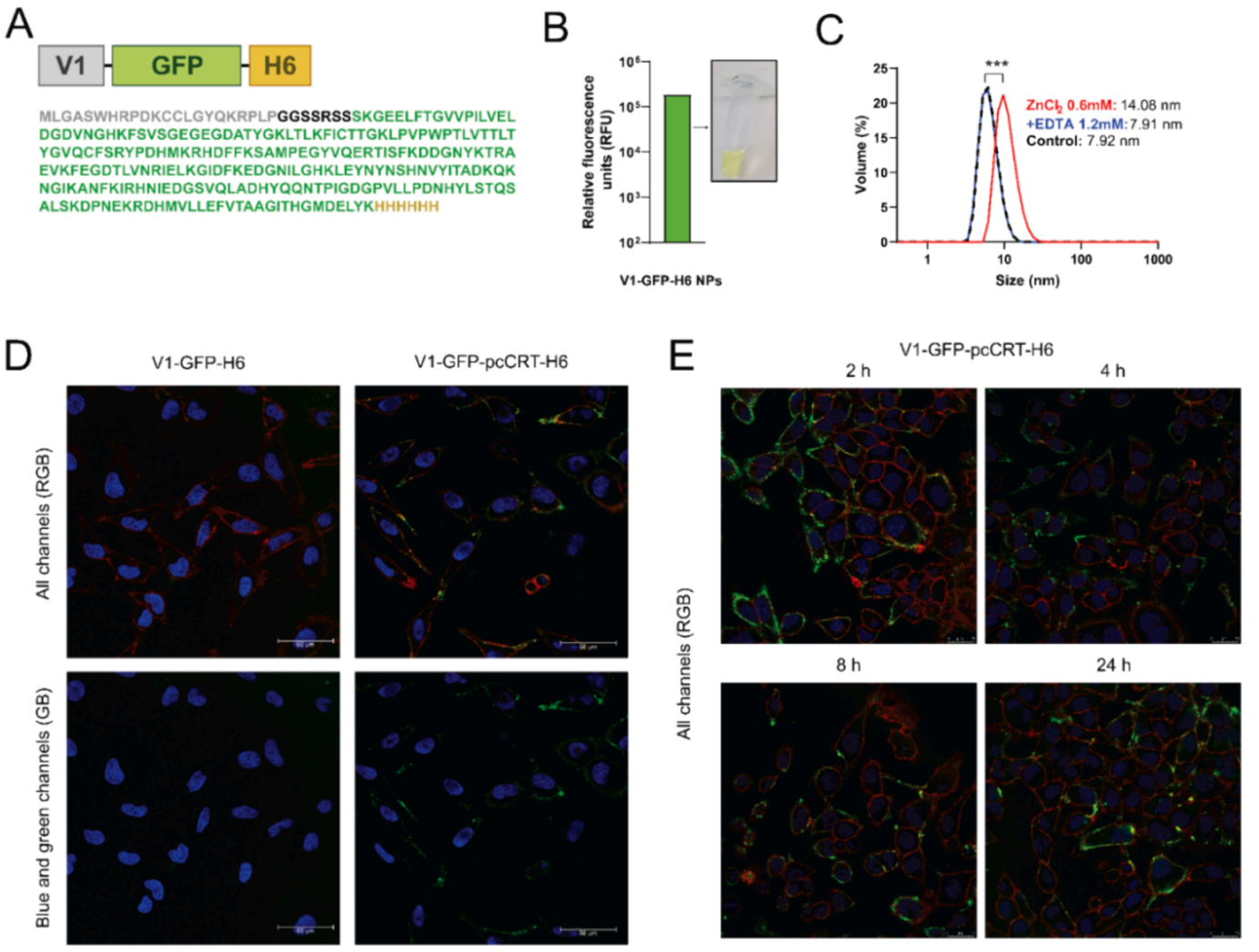

Fig. 3. Description of V1-GFP-H6 and cell binding characterization of the modular proteins. A. Modular organization and amino acid sequence of V1-GFP-H6. B. Straightforward fluorescent emission (510–580 nm) of the assembled protein upon excitation with blue LED light (430–495 nm) in comparison to a non-fluorescent protein. The inset provides visual proof of the protein fluorescence. C. Volume-size distribution and mean size determination via DLS of the recombinant V1-GFP-H6 in unassembled (black), Zn-assembled (red) and EDTA-disassembled (blue) forms. Differences between the peak size values of assembled and unassembled samples are statistically significant (***; $p < 0.001$). D. Distribution of V1-GFP-H6 and V1-GFP-pcCRT-H6 nanoparticles in CXCR4$^+$ HeLa cells determined by confocal microscopy after exposure to 2 μM of the materials for 2 h. E. Distribution of V1-GFP-pcCRT-H6 nanoparticles after exposure to 2 μM of the materials after 2, 4, 8 and 24 h. The nuclei were stained in blue with Hoechst, the plasma membranes were stained in red with CellMask™ and the green staining corresponds to the GFP-containing constructs.

deviation (SD). All measurements were performed at least in triplicates except for cytometry, which was performed using duplicates.

3. Results

Among the tested peptide ligands of the tumoral marker CXCR4, V1, a derivative from the herpesvirus chemokine vMIP-II [43] showed antagonistic CXCR4 activities that prevented HIV cell infection, among other CXCR4-dependent activities [43], but with undetectable internalization into CXCR4$^+$ cells [25]. This fact prompted us to explore such ligand as a tool to promote CXCR4$^+$ cell surface tagging with a desired protein. Then, the modular V1-GFP-pcCRT-H6 protein was constructed (Fig. 1A) and produced in *E. coli* in a recombinant form. The fusion protein was intended to contain V1 as a targeting agent, a functional CRT version (harboring the P and C domains) as a tag, GFP as a monitoring agent, and a hexahistidine tail (H6) to allow purification from recombinant bacteria and to promote cation-assisted self-assembling as oligomeric nanoparticles [44]. The N-terminus of CRT was substituted with GFP based on findings by Wijeyesakere SJ et al. [45], which showed that the P and C domains are essential for CRT's function in activating macrophages, whereas the N-domain can be replaced without losing this functionality. Substituting the N-domain with GFP was necessary to avoid the complications of having a construct that includes both full-length CRT and GFP, which would be large, complex, and likely prone to misfolding [44]. Indeed, the soluble protein was fluorescent (Fig. 1B), and it showed a hydrodynamic size of 12 nm that was increased to around 16 nm by the addition of cationic Zn (Fig. 1C). The divalent Zn^{2+} acts as intermolecular gluing agent for H6-tagged proteins, that promotes protein oligomerization within the nanoscale [46]. As expected, the oligomeric status was fully reversed upon the addition of the chelating agent EDTA (Fig. 1C).

In a preliminary screening (Fig. 2A), V1-GFP-pcCRT-H6 was intravenously administered, via tail vein, in a subcutaneous (SC) mouse model bearing CXCR4$^+$ leukemic cells. V1 being a ligand of CXCR4, we expected to observe accumulation of GFP fluorescence in tumor a few hours after administration much over the control protein, as it occurred with other CXCR4-targeted nanoparticles empowered with the alternative peptidic ligands of CXCR4, namely T22 [47] or EPIX4 [26]. Indeed,

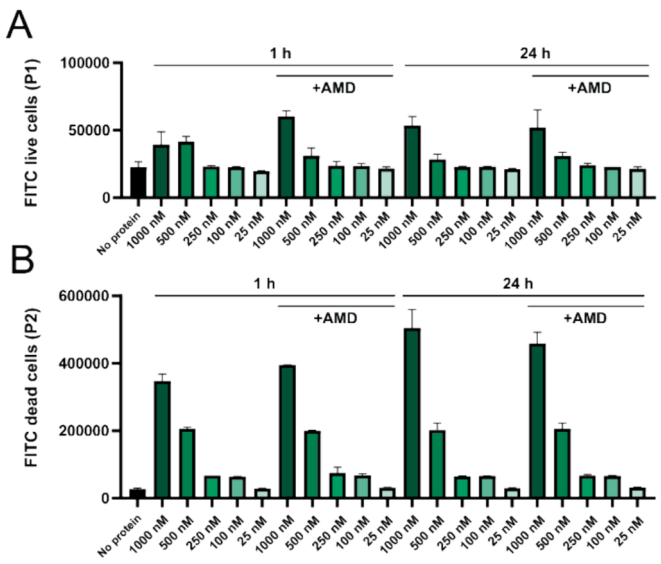

Fig. 4. Cell binding specificity of V1-GFP-pcCRT-H6 to THP-1 cells. Green (FITC) fluorescence of live cells (A) or death cells (B) by flow cytometry after exposure to V1-GFP-pcCRT-H6 nanoparticles at increasing concentrations for 1 and 24 h. The CXCR4 antagonist AMD3100 was added to the cell culture 1 h before the protein addition to test competitive binding.

a modest tumor accumulation was observed (Fig. 2B) but surprisingly, the fluorescence was not exclusively found in tumor tissues, and it was also present as background in other organs. This fact was indicative of a moderate precision in the CXCR4-targeted GFP labelling compared to previous biodistribution analyses of the alternative CXCR4 ligand T22 [25,37].

While the antagonistic activities of V1 over CXCR4 had been well described [43], the selective binding of V1 to CXCR4 and the biodistribution of V1-empowered materials such as nanoparticles had been not precisely determined. In this context, and to finely dissect the targeting abilities of V1, we constructed V1-GFP-H6 (Fig. 3A), that assembled as fluorescent nanoparticles (Fig. 3B) of around 14 nm (Fig. 3C) upon Zn^{2+} addition. When exposed to $CXCR4^{+}$ HeLa cells, V1-GFP-H6 was unable to label them (Fig. 3D). This contrasted with V1-GFP-pcCRT-H6, that efficiently labeled cultured cells (Fig. 3D) without detectable internalization up to 24 h after incubation (Fig. 3E). These data indicate that the cell binding capabilities and consequent biodistribution of V1-GFP-pcCRT-H6 could be mediated by CRT rather than by V1, since V1 alone promotes limited cell adhesion, if any, while the addition of the CRT domain to the construct enables such protein-cell interaction. Also, the absence of internalization results in a very stable cell labelling, in this particular case with GFP.

To explore further this possibility, we tested how a CXCR4 chemical antagonist, namely AMD3100 [30,48,49], could prevent the binding of V1-GFP-pcCRT-H6 to cells. Indeed, AMD3100 efficiently blocks cell binding and penetrability of other previously tested ligands of CXCR4 such as T22 and EPIX4, both in vitro [25] and in vivo [50] and serves as a robust method to assess the specificity of protein binding to CXCR4, having demonstrated its efficacy in CXCR4 + cell lines across various reference studies [34,36,42].

As observed (Fig. 4A), AMD3100 did not interfere with the cell binding properties of V1-GFP-pcCRT-H6, suggesting that the observed cell adhesion properties are irrespective of the pair V1/CXCR4. This fact, in agreement with the lack of cell interactivity of V1-GFP-H6 (Fig. 3), indicates that the capability of V1 to bind CXCR4 is moderate and overcome by alternative binding properties of the whole construct. Despite this fact, the capability of cell binding by V1-GFP-pcCRT-H6 was clearly enhanced when analyzing the dead cells population (Fig. 4B). In any case, AM3100 was always non effective over V1-GFP-pcCRT-H6, while this chemical was fully competent in preventing the CXCR4-specific cell binding of T22-GFP-H6 (Fig. 5A). In this sense, T22-dependent binding is also linked to a subsequent internalization [25], while the observed binding of the V1-GFP-pcCRT-H6 construct to cells did not lead to such outcome (Fig. 3D, E and Fig. 6D). Also, the avidity of T22 for dead cells was only moderate in contrast to V1-GFP-pcCRT-H6 at increasing concentrations (Fig. 5B), in agreement with data from Fig. 4A and B. This fact indicated that the preferential binding of V1-GFP-pcCRT-H6 to dead cells that we had inferred from Fig. 4 was not an artifact, that is, it was not caused by a nonspecifically enhanced adsorption of any protein to senescent cells but by a specific interaction mediated by CRT. The data presented above were suggestive of CRT conferring to modular proteins cell binding activities stronger than those that V1 might offer, and irrespective of CXCR4. This was obvious from the fact that the only difference between the binder V1-GFP-pcCRT-H6 and the non-binder V1-GFP-H6 was the occurrence of the CRT domain. To further explore this fact and confirm the concept, we constructed a non-fluorescent version of the modular CRT, namely V1-CRT-H6 (Fig. 6A). This protein harbored all three main domains of calreticulin (i.e. N, P, and C domains) and was also capable of self-assembly (Fig. 6B) in presence of Zn^{2+} but it was not fluorescent (Fig. 6C). Then, in absence of fluorescence emission, it was used as a competitor for the binding of V1-GFP-pcCRT-H6 to $CXCR4^{+}$ HeLa cells. As

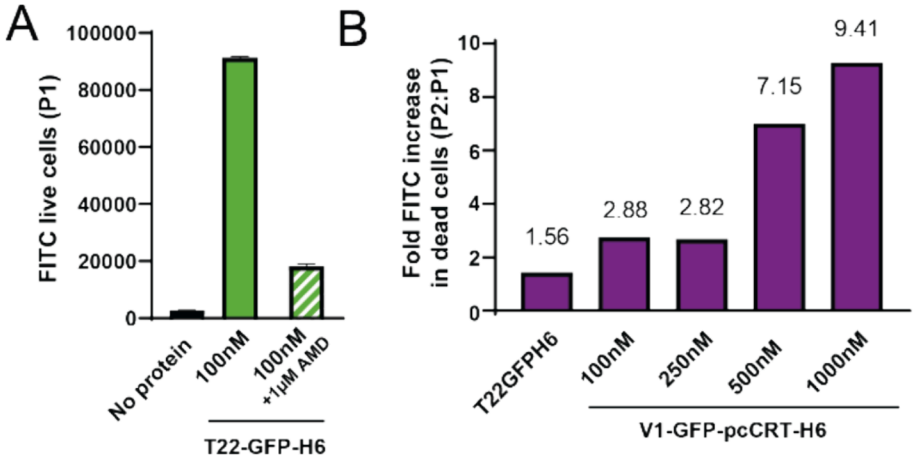

Fig. 5. A. Cell binding specificity of T22-GFP-H6, used as a positive control to demonstrate CXCR4 receptor-dependent internalization, that can be reverted upon addition of the CXCR4 antagonist AMD3100. B. Fold increase in fluorescence of T22-GFP-H6 (100 nM) and V1-GFP-pcCRT-H6 (100–1000 nM) proteins comparing levels detected in the THP-1 live or dead cells fractions in flow cytometry.

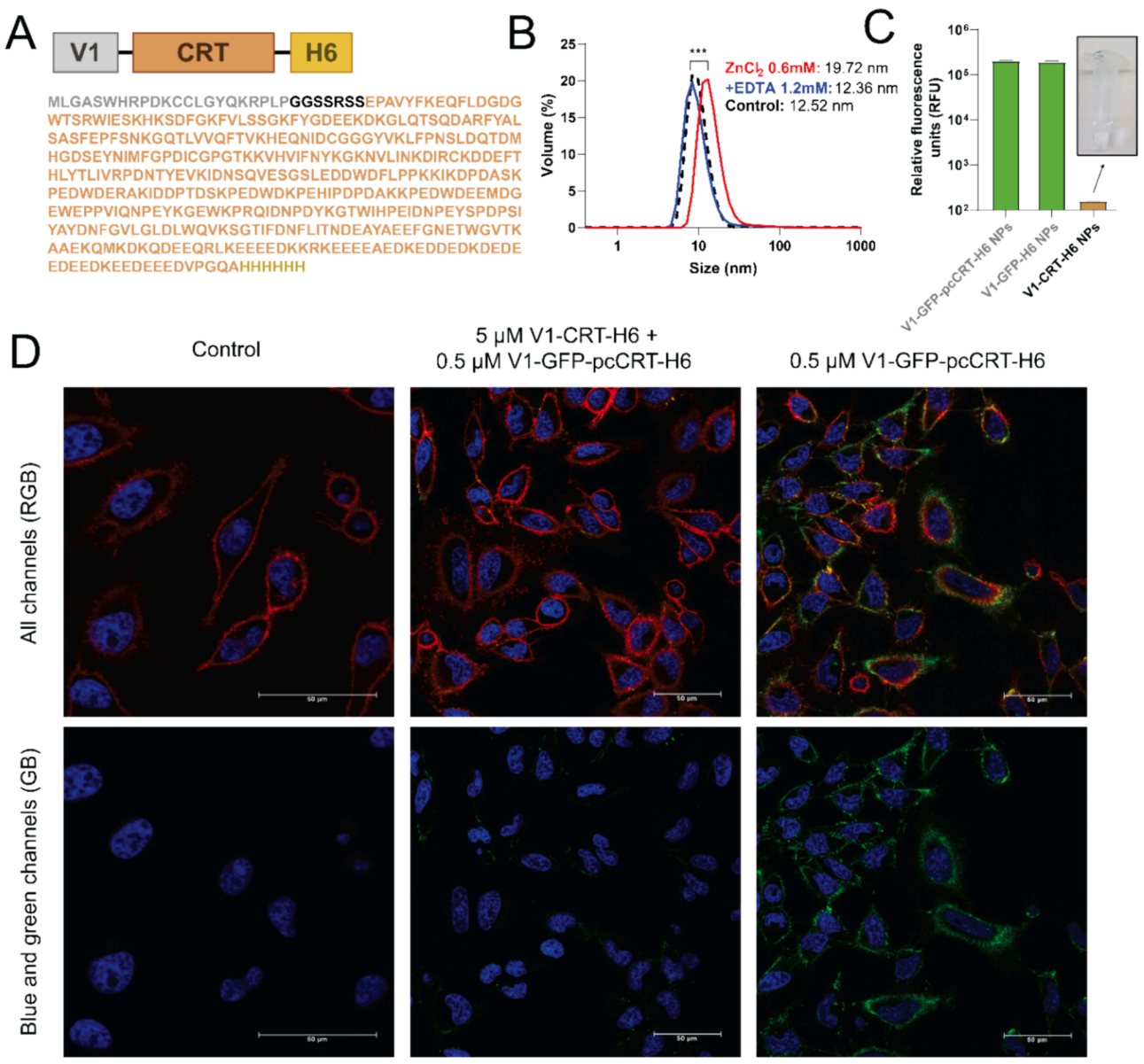

Fig. 6. Description and characterization of V1-CRT-H6. A. Modular organization and amino acid sequence of V1-CRT-H6. B. Volume-size distribution and mean size determination via DLS of the recombinant V1-CRT-H6 in unassembled (red), Zn-assembled (black) and EDTA-disassembled (blue) forms. Differences between the peak size values of assembled and unassembled samples are statistically significant (***; $p < 0.001$). C. Relative fluorescence, that indicates the lack of green fluorescence emission (510–580 nm) of the assembled protein upon excitation with blue LED light (430–495 nm). The inset provides visual proof of the lack of fluorescent emission of the protein solution. D. Distribution of V1-GFP-pcCRT-H6 nanoparticles (500 nM) in CXCR4$^+$ HeLa cells (control, left panel) by confocal microscopy after 2 h incubation with (central panel) and without (right panel) competitor (V1-CRT-H6) pre-incubated 1 h at 5 µM. Nucleus were stained in blue with Hoechst, plasma membranes were stained in red with CellMask™ and green staining corresponds to the GFP-containing constructs.

observed, the non-fluorescent protein version could inhibit the cell binding of V1-GFP-pcCRT-H6 (Fig. 6D).

This finding fully confirmed previous data in Fig. 3 and the assumption that CRT (and not V1) was the protein domain driving the cell binding of V1-GFP-pcCRT-H6 by a mechanism independent of CXCR4.

4. Discussion

CRT is a cytosolic chaperone with multiple cellular functions that under stress conditions or during programmed cell death migrates to the cell surface. In the early stages of cell death or in pre-apoptotic cells, CRT is externalized [17,51–53], promoting the phagocytic clearance of death cells. Labelling or over-labelling the surface of tumor cells with CRT would be then a way to precisely stimulate immunogenic tumor destruction [54], in form of a novel immune-based synergistic cancer treatment. The peptide V1, a ligand of the tumoral marker CXCR4 [43] was used here to drive the in vivo delivery of a recombinant CRT (Fig. 1) to CXCR4$^+$ cancer cells in absence of internalization [25]. However, it failed to render a standard biodistribution of the injected protein in a subcutaneous mouse model of CXCR4$^+$ cancer (Fig. 2). The unexpected low level of selectiveness and accumulation of the protein in tumor tissues was in contrast with the very precise targeting previously observed in the delivery of proteins and protein nanoparticles to several cancer models, when using an alternative CXCR4 ligand, the peptide T22 [25,34].

In fact, V1 showed here very poor (almost undetectable) levels of cell binding (Fig. 3). Actually, its affinity for CXCR4 is between 1 and 2 orders of magnitude lower than that of the parental cytokine vMIP-II [43]. Despite this, the peptide has been described as a potent CXCR4

antagonist that efficiently inhibits CXCR4-dependent HIV infection and cell migration [43]. The capability of the protein V1-GFP-H6 to bind cells is instead conferred by CRT (Fig. 3), in a fully CXCR4-independent fashion, being such activity preferential over the dead cells population as discriminated by the flow cytometer (Fig. 4). This preferred dead cell binding is not shown by the construct T22-GFP-H6 (Fig. 5), which demonstrates that it is not an artifactual issue but an active mechanism. The supposed CRT-mediated cell binding blockage by an excess of CRT (Fig. 6) confirms that this protein is involved in the superficial cell binding of V1-GFP-pcCRT-H6. In contrast to the T22-GFP-H6 construct, which promotes both cell binding and internalization through the well-characterized CXCR4 pathway [25], the CRT-based nanoparticles exhibit surface binding without subsequent internalization (Fig. 3).The way in which nanostructured CRT attach cells and preferentially, dead cells, needs further investigation. However, it is known that this protein tends to self-oligomerize [55–57] and, on the other hand, it abounds on the dying cell surface [17,51–53]. Additionally, we discarded the possibility that the HeLa cells observed in confocal microscopy labeled with V1-GFP-pcCRT-H6 were already dead, as there were no morphological changes indicative of cell death. This reinforces that V1-GFP-pcCRT-H6 binding does not necessarily indicate cell death but may reflect the presence of ecto-calreticulin on the cell surface, which can act as an "eat-me" signal under stress conditions [58].

Combining these facts and the observations presented here, a specific interaction between the soluble and the cell-surface exposed CRT could not be discarded. Such interaction could be enhanced by the multimeric nature of the soluble CRT (Fig. 1), since the multivalent display of ligands promotes cooperativity and tighter and highly selective binding through cell surface interactors [59,60]. We also considered the possibility of THP-1 behaving as macrophages and conducting phagocytosis to induced by CRT binding to targeted cells. However, this scenario would likely result in the degradation or consumption of the V1-GFP-pcCRT-H6 construct, leading to a lack of observable fluorescence. Additionally, if THP1 cells were phagocytized after initial binding, they would be ingested by macrophages and not appear as distinct events in the P2 population during cytometry.

Irrespective of the precise mechanics, targeting senescent or dying cells is a promising therapeutic approach in diverse clinical fields, including aging, regenerative medicine, and vascular diseases [61–66], specially aiming at the destruction of such target cells. The novel cell-targeting properties of CRT described here provide a new tool among those available in such approaches, offering an effective ligand that enjoys from the versatility, manipulability, and easy productivity of recombinant proteins.

5. Conclusions

A recombinant calreticulin, incorporated into multidomain protein-only nanoparticles, surpasses the targeting properties of an accompanying CXCR4 ligand V1, a fragment of the viral cytokine vMIP-II. The protein, initially intended as a surface 'eat-me' signal for cancer cells, shows specificity for senescent cells, through a stable and specific interaction that is inhibited by soluble calreticulin and that does not result in efficient cell uptake. Being an unexpected data, the possibility of targeting dying cells by means of protein-only nanoparticles offers a new strategy for their selective labelling and drug delivery. This possibility is critical in fields such as regenerative medicine and ageing that are under the imperative need of new diagnostic, therapeutic and theragnostic approaches.

Author contributions

Parladé E designed the recombinant proteins and performed in vitro studies, with the support of Voltà-Durán E and Unzueta U; García-Leon A and Casanova I performed the biodistribution assays; Villaverde A, Mangues R and Vázquez E acquired the financial support; Villaverde A wrote the paper with support from Parladé E. All authors contributed to the general discussion.

CRediT authorship contribution statement

Eloi Parladé: Writing – review & editing, Writing – original draft, Visualization, Software, Project administration, Methodology, Investigation, Formal analysis, Conceptualization. **Annabel García-Leon:** Writing – review & editing, Methodology, Investigation. **Eric Voltà-Durán:** Writing – review & editing, Methodology, Investigation. **Ugutz Unzueta:** Writing – review & editing, Methodology, Investigation. **Ramon Mangues:** Writing – review & editing, Funding acquisition. **Isolda Casanova:** Writing – review & editing, Investigation. **Antonio Villaverde:** Writing – review & editing, Writing – original draft, Funding acquisition, Conceptualization. **Esther Vázquez:** Writing – review & editing, Funding acquisition.

Declaration of Competing Interest

The authors declare that they have no known competing financial interests or personal relationships that could have appeared to influence the work reported in this paper.

Data availability

Data is available at https://doi.org/10.34810/data1055.

Acknowledgements

The authors appreciate the financial support received for the development of multimeric recombinant drugs, from AEI (PID2022-136845OB-I00 financed by MCIN/AEI/10.13039/501100011033 to E. V. & A.V. and PID2020-116174RB-I00 to A.V.), AGAUR (SGR2021-00092 to A.V. SGR-CatM.2021-01140 to R.M.), Instituto de Salud Carlos III (PI20/00400 and PI23/00318 to U.U.) co-funded by European Regional Development Fund (ERDF, a way to make Europe). We also appreciate the funding from the CIBER –Consorcio Centro de Investigación Biomédica en Red– (CB06/01/0014 and CB06/01/1031) through TRACC and TRAILS intramural projects (to E.P.), Instituto de Salud Carlos III, Ministerio de Ciencia e Innovación, through the project PI21/00150 to R.M. A.V. received an ICREA ACADEMIA award. The authors are indebted to the Nanotoxicology Unit of the ICTS-141007 Nanbiosis Platform (http://www.nanbiosis.es/portfolio/u18-nanotoxicology-unit/) for the in vivo work. Protein production was partially performed by the ICTS "NANBIOSIS", more specifically by the Protein Production Platform of CIBER in Bioengineering, Biomaterials & Nanomedicine (CIBER-BBN)/ IBB, at the UAB (http://www.nanbiosis.es/portfolio/u1-protein-production-platform-ppp/). E.V.D was supported by a predoctoral fellowship from Ministerio de Ciencia, Innovación y Universidades (FPU18/04615). UU was supported by Miguel Servet contract (CP19/00028) from ISCIII co-funded by European Social Fund (ESF investing in your future). Cell culture and cytometry experiments were performed at SCAC facilities in the UAB. Confocal microscopy studies were performed at the Servei de Microscòpia in the UAB.

Appendix A. Supplementary data

Supplementary data to this article can be found online at https://doi.org/10.1016/j.ejpb.2024.114410.

References

[1] V. Schirrmacher, From chemotherapy to biological therapy: a review of novel concepts to reduce the side effects of systemic cancer treatment (Review), Int. J. Oncol. 54 (2019), https://doi.org/10.3892/ijo.2018.4661.

[2] K. Bukowski, M. Kciuk, R. Kontek, Mechanisms of multidrug resistance in cancer chemotherapy, Int. J. Mol. Sci. 21 (9) (2020) 3233, https://doi.org/10.3390/ijms21093233.
[3] J. Baselga, D.M. Hyman, A view on drug resistance in cancer, Nature 575 (7782) (2019) 299–309, https://doi.org/10.1038/s41586-019-1730-1.
[4] J.L. Stow, Y. Hung, A.A. Wall, Macropinocytosis: Insights from immunology and cancer, Curr. Opin. Cell Biol. 65 (2020) 131–140, https://doi.org/10.1016/j.ceb.2020.06.005.
[5] K.J. Hiam-Galvez, B.M. Allen, M.H. Spitzer, Systemic immunity in cancer, Nat. Rev. Cancer 21 (6) (2021) 345–359, https://doi.org/10.1038/s41568-021-00347-z.
[6] S.L. Meier, A.T. Satpathy, D.K. Wells, Bystander T cells in cancer immunology and therapy, Nat. Cancer 3 (2) (2022) 143–155, https://doi.org/10.1038/s43018-022-00335-8.
[7] J. Borst, T. Ahrends, N. Bąbała, C.J. Melief, W. Kastenmüller, CD4+ T cell help in cancer immunology and immunotherapy, Nat. Rev. Immunol 18 (10) (2018) 635–647, https://doi.org/10.1038/s41577-018-0044-0.
[8] F. Chen, Y. Wang, J. Gao, M. Saeed, T. Li, W. Wang, H. Yu, Nanobiomaterial-based vaccination immunotherapy of cancer, Biomater 270 (2021) 120709, https://doi.org/10.1016/j.biomaterials.2021.120709.
[9] N. Erfanian, A. Derakhshani, S. Nasseri, M. Fereidouni, B. Baradaran, N.J. Tabrizi, O. Brunetti, R. Bernardini, N. Silvestris, H. Safarpour, Immunotherapy of cancer in single-cell RNA sequencing era: A precision medicine perspective, Biomed. Pharmacother 146 (2022) 112558, https://doi.org/10.1016/j.biopha.2021.112558.
[10] S. Lorenzo-Herrero, A. López-Soto, C. Sordo-Bahamonde, A.P. Gonzalez-Rodriguez, M. Vitale, S. Gonzalez, NK cell-based immunotherapy in cancer metastasis, Cancers 11 (1) (2018) 29, https://doi.org/10.3390/cancers11010029.
[11] L. Kraehenbuehl, C.H. Weng, S. Eghbali, J.D. Wolchok, T. Merghoub, Enhancing immunotherapy in cancer by targeting emerging immunomodulatory pathways, Nat. Rev. Clin. Oncol. 19 (1) (2022) 37–50, https://doi.org/10.1038/s41571-021-00552-7.
[12] S. Gu, T. Ni, J. Wang, Y. Liu, Q. Fan, Y. Wang, T. Huang, Y. Chu, X. Sun, Y. Wang, CD47 Blockade Inhibits Tumor Progression through Promoting Phagocytosis of Tumor Cells by M2 Polarized Macrophages in Endometrial Cancer, J Immunol Res (2018), https://doi.org/10.1155/2018/6156757.
[13] C.M. Schürch, M.A. Roelli, S. Forster, M.H. Wasmer, F. Brühl, R.S. Maire, S. Di Pancrazio, M.D. Ruepp, R. Giger, A. Perren, A.M. Schmitt, P. Krebs, R.P. Charles, M.S. Dettmer, Targeting CD47 in anaplastic thyroid carcinoma enhances tumor phagocytosis by macrophages and is a promising therapeutic strategy, Thyroid 29 (2019), https://doi.org/10.1089/thy.2018.0555.
[14] D.V. Krysko, K.S. Ravichandran, P. Vandenabeele, Macrophages regulate the clearance of living cells by calreticulin, Nat. Commun 9 (1) (2018) 4644, https://doi.org/10.1038/s41467-018-06807-9.
[15] M. Feng, K.D. Marjon, F. Zhu, R. Weissman-Tsukamoto, A. Levett, K. Sullivan, K. S. Kao, M. Markovic, P.A. Bump, H.M. Jackson, T.S. Choi, J. Chen, A.M. Banuelos, J. Liu, P. Gip, L. Cheng, D. Wang, I.L. Weissman, Programmed cell removal by calreticulin in tissue homeostasis and cancer, Nat. Commun. 9 (2018), https://doi.org/10.1038/s41467-018-05211-7.
[16] A. Schcolnik-Cabrera, B. Oldak, M. Juárez, M. Cruz-Rivera, A. Flisser, F. Mendlovic, Calreticulin in phagocytosis and cancer: opposite roles in immune response outcomes, Apoptosis 24 (2019) 245–255, https://doi.org/10.1007/s10495-019-01532-0.
[17] I. Martins, O. Kepp, L. Galluzzi, L. Senovilla, F. Schlemmer, S. Adjemian, L. Menger, M. Michaud, L. Zitvogel, G. Kroemer, Surface-exposed calreticulin in the interaction between dying cells and phagocytes, Ann. N. Y. Acad. Sci. 1209 (2010), https://doi.org/10.1111/j.1749-6632.2010.05740.x.
[18] D.V. Krysko, A.D. Garg, A. Kaczmarek, O. Krysko, P. Agostinis, P. Vandenabeele, Immunogenic cell death and DAMPs in cancer therapy, Nat. Rev. Cancer 12 (12) (2012) 860–875, https://doi.org/10.1038/nrc3380.
[19] A.D. Garg, P. Agostinis, Cell death and immunity in cancer: from danger signals to mimicry of pathogen defense responses, Immunol. Rev. 280 (1) (2017) 126–148, https://doi.org/10.1111/imr.12574.
[20] S.M. Kelley, K.S. Ravichandran, Putting the brakes on phagocytosis: "don't-eat-me" signaling in physiology and disease, EMBO Rep. 22 (2021), https://doi.org/10.15252/embr.202152564.
[21] M.P. Chao, S. Jaiswal, R. Weissman-Tsukamoto, A.A. Alizadeh, A.J. Gentles, J. Volkmer, K. Weiskopf, S.B. Willingham, T. Raveh, C.Y. Park, R. Majeti, I. L. Weissman, Calreticulin is the dominant pro-phagocytic signal on multiple human cancers and is counterbalanced by CD47, Sci. Transl. Med. 2 (2010), https://doi.org/10.1126/scitranslmed.3001375.
[22] R. Uger, L. Johnson, Blockade of the CD47-SIRPα axis: a promising approach for cancer immunotherapy, Expert Opin. Biol. Ther. 20 (1) (2020) 5–8, https://doi.org/10.1080/14712598.2020.1685976.
[23] J. Kim, S. Sinha, M. Solomon, E. Perez-Herrero, J. Hsu, Z. Tsinas, S. Muro, Co-coating of receptor-targeted drug nanocarriers with anti-phagocytic moieties enhances specific tissue uptake versus non-specific phagocytic clearance, Biomaterials 147 (2017), https://doi.org/10.1016/j.biomaterials.2017.08.045.
[24] K. Weiskopf, N.S. Jahchan, P.J. Schnorr, S. Cristea, A.M. Ring, R.L. Maute, A. K. Volkmer, J.P. Volkmer, J. Liu, J.S. Lim, D. Yang, G. Seitz, T. Nguyen, D. Wu, K. Jude, H. Guerston, A. Barkal, F. Trapani, J. George, J.T. Poirier, E.E. Gardner, L. A. Miles, E. De Stanchina, S.M. Lofgren, H. Vogel, M.M. Winslow, C. Dive, R. K. Thomas, C.M. Rudin, M. Van De Rijn, R. Majeti, K.C. Garcia, I.L. Weissman, J. Sage, CD47-blocking immunotherapies stimulate macrophage-mediated destruction of small-cell lung cancer, J. Clinic. Invest. 126 (2016), https://doi.org/10.1172/JCI81603.
[25] U. Unzueta, M.V. Céspedes, N. Ferrer-Miralles, I. Casanova, J. Cedano, J. L. Corchero, J. Domingo-Espín, A. Villaverde, R. Mangues, E. Vázquez, Intracellular CXCR4+ cell targeting with T22-empowered protein-only nanoparticles, Int. J. Nanomed. 7 (2012) 4533–4544, https://doi.org/10.2147/IJN.S34450.
[26] O. Cano-Garrido, P. Álamo, L. Sánchez-García, A. Falgàs, A. Sánchez-Chardi, N. Serna, E. Parladé, U. Unzueta, M. Roldán, E. Voltà-Durán, I. Casanova, A. Villaverde, R. Mangues, E. Vázquez, Biparatopic protein nanoparticles for the precision therapy of cxcr4+ cancers, Cancers (basel). 13 (2021), https://doi.org/10.3390/cancers13122929.
[27] J.Y. Lee, D.H. Kang, D.Y. Chung, J.K. Kwon, H. Lee, N.H. Cho, Y.D. Choi, S.J. Hong, K.S. Cho, Meta-analysis of the relationship between CXCR4 expression and metastasis in prostate cancer, World J Mens Health. 32 (2014), https://doi.org/10.5534/wjmh.2014.32.3.167.
[28] Z. Zhang, C. Ni, W. Chen, P. Wu, Z. Wang, J. Yin, J. Huang, F. Qiu, Expression of CXCR4 and breast cancer prognosis: A systematic review and meta-analysis, BMC Cancer 14 (2014), https://doi.org/10.1186/1471-2407-14-49.
[29] C.F. Liu, S.Y. Liu, X.Y. Min, Y.Y. Ji, N. Wang, D. Liu, N. Ma, Z.F. Li, K. Li, The prognostic value of CXCR4 in ovarian cancer: a meta-analysis, PLoS One 9 (2014), https://doi.org/10.1371/journal.pone.0092629.
[30] H.-Y. Kim, J.-Y. Hwang, S.-W. Kim, H.-J. Lee, H.-J. Yun, S. Kim, D.-Y. Jo, The CXCR4 antagonist AMD3100 has dual effects on survival and proliferation of myeloma cells in vitro, Cancer Res. Treat. 42 (2010), https://doi.org/10.4143/crt.2010.42.4.225.
[31] J.M. Busillo, J.L. Benovic, Regulation of CXCR4 signaling, Biochim. Biophys. Acta - Biomembr 1768 (4) (2007) 952–963, https://doi.org/10.1016/j.bbamem.2006.11.002.
[32] N. Serna, V. Pallarès, U. Unzueta, A. Garcia-Leon, E. Voltà-Durán, A. Sánchez-Chardi, E. Parladé, A. Rueda, I. Casanova, A. Falgàs, L. Alba-Castellón, J. Sierra, A. Villaverde, E. Vázquez, R. Mangues, Engineering non-antibody human proteins as efficient scaffolds for selective, receptor-targeted drug delivery, J. Control. Release 343 (2022), https://doi.org/10.1016/j.jconrel.2022.01.017.
[33] N. Serna, J.V. Carratalá, O. Conchillo-Solé, C. Martínez-Torró, U. Unzueta, R. Mangues, N. Ferrer-Miralles, X. Daura, E. Vázquez, A. Villaverde, Antibacterial activity of t22, a specific peptidic ligand of the tumoral marker cxcr4, Pharmaceutics. 13 (2021), https://doi.org/10.3390/pharmaceutics13111922.
[34] M.V. Céspedes, U. Unzueta, A. Aviñó, A. Gallardo, P. Álamo, R. Sala, A. Sánchez-Chardi, I. Casanova, M.A. Mangues, A. Lopez-Pousa, R. Eritja, A. Villaverde, E. Vázquez, R. Mangues, Selective depletion of metastatic stem cells as therapy for human colorectal cancer, EMBO Mol. Med. (2018), https://doi.org/10.15252/emmm.201708772.
[35] N. Serna, A. Falgàs, A. García-León, U. Unzueta, Y. Núñez, A. Sánchez-Chardi, C. Martínez-Torró, R. Mangues, E. Vazquez, I. Casanova, A. Villaverde, Time-prolonged release of tumor-targeted protein–MMAE nanoconjugates from implantable hybrid materials, Pharmaceutics. 14 (2022), https://doi.org/10.3390/pharmaceutics14010192.
[36] V. Pallarès, U. Unzueta, A. Falgàs, A. Aviñó, Y. Núñez, A. García-León, L. Sánchez-García, N. Serna, A. Gallardo, L. Alba-Castellón, P. Álamo, J. Sierra, L. Cedó, R. Eritja, A. Villaverde, E. Vázquez, I. Casanova, R. Mangues, A multivalent Ara-C-prodrug nanoconjugate achieves selective ablation of leukemic cells in an acute myeloid leukemia mouse model, Biomaterials 280 (2022), https://doi.org/10.1016/j.biomaterials.2021.121258.
[37] R. Díaz, V. Pallarès, O. Cano-Garrido, N. Serna, L. Sánchez-García, A. Falgàs, M. Pesarrodona, U. Unzueta, A. Sánchez-Chardi, J.M. Sánchez, I. Casanova, E. Vázquez, R. Mangues, A. Villaverde, Selective CXCR4^{+}cancer cell targeting and potent antineoplastic effect by a nanostructured version of recombinant ricin, Small 14 (2018), https://doi.org/10.1002/smll.201800665.
[38] E. Voltà-Durán, N. Serna, L. Sánchez-García, A. Aviñó, J.M. Sánchez, H. López-Laguna, O. Cano-Garrido, I. Casanova, R. Mangues, R. Eritja, E. Vázquez, A. Villaverde, U. Unzueta, Design and engineering of tumor-targeted, dual-acting cytotoxic nanoparticles, Acta Biomater. 119 (2021), https://doi.org/10.1016/j.actbio.2020.11.018.
[39] L. Sánchez-García, R. Sala, N. Serna, P. Álamo, E. Parladé, L. Alba-Castellón, E. Voltà-Durán, A. Sánchez-Chardi, U. Unzueta, E. Vázquez, R. Mangues, A. Villaverde, A refined cocktailing of pro-apoptotic nanoparticles boosts anti-tumor activity, Acta Biomater. 113 (2020), https://doi.org/10.1016/j.actbio.2020.06.033.
[40] E. Rioja-Blanco, I. Arroyo-Solera, P. Álamo, I. Casanova, A. Gallardo, U. Unzueta, N. Serna, L. Sánchez-García, M. Quer, A. Villaverde, E. Vázquez, X. León, L. Alba-Castellón, R. Mangues, CXCR4-targeted nanotoxins induce GSDME-dependent pyroptosis in head and neck squamous cell carcinoma, J. Experim. Clinical Cancer Res. 41 (2022), https://doi.org/10.1186/s13046-022-02267-8.
[41] R. Sala, E. Rioja-Blanco, N. Serna, L. Sánchez-García, P. Álamo, L. Alba-Castellón, I. Casanova, A. López-Pousa, U. Unzueta, M.V. Céspedes, E. Vázquez, A. Villaverde, R. Mangues, GSDMD-dependent pyroptotic induction by a multivalent CXCR4-targeted nanotoxin blocks colorectal cancer metastases, Drug Deliv. 29 (2022), https://doi.org/10.1080/10717544.2022.2069302.
[42] V. Pallarès, U. Unzueta, A. Falgàs, L. Sánchez-Garciá, N. Serna, A. Gallardo, G. A. Morris, L. Alba-Castellón, P. Álamo, J. Sierra, A. Villaverde, E. Vázquez, I. Casanova, R. Mangues, An Auristatin nanoconjugate targeting CXCR4+ leukemic cells blocks acute myeloid leukemia dissemination, J. Hematol. Oncol. 13 (2020), https://doi.org/10.1186/s13045-020-00863-9.
[43] N. Zhou, Z. Luo, J. Luo, J.W. Hall, Z. Huang, A novel peptide antagonist of CXCR4 derived from the N-terminus of viral chemokine vMIP-II, Biochemistry 39 (2000), https://doi.org/10.1021/bi992750v.
[44] H. López-Laguna, E. Voltà-Durán, E. Parladé, A. Villaverde, E. Vázquez, U. Unzueta, Insights on the emerging biotechnology of histidine-rich peptides,

Biotechnol. Adv. 54 (2022) 107817, https://doi.org/10.1016/J.BIOTECHADV.2021.107817.
[45] S.J. Wijeyesakere, S.K. Bedi, D. Huynh, M. Raghavan, The C-terminal acidic region of calreticulin mediates phosphatidylserine binding and apoptotic cell phagocytosis, J. Immunol. 196 (2016) 3896–3909, https://doi.org/10.4049/JIMMUNOL.1502122.
[46] H. López-Laguna, J. Sánchez, U. Unzueta, R. Mangues, E. Vázquez, A. Villaverde, Divalent cations: a molecular glue for protein materials trends in biochemical sciences an official publication of the international union of biochemistry and molecul ar biology, Trends Biochem. Sci 45 (2020), https://doi.org/10.1016/j.tibs.2020.08.003.
[47] N. Serna, M.V. Céspedes, L. Sánchez-García, U. Unzueta, R. Sala, A. Sánchez-Chardi, F. Cortés, N. Ferrer-Miralles, R. Mangues, E. Vázquez, A. Villaverde, Peptide-based nanostructured materials with intrinsic proapoptotic activities in CXCR4^{+}solid tumors, Adv. Funct. Mater. 27 (2017), https://doi.org/10.1002/adfm.201700919.
[48] E. De Clercq, AMD3100/CXCR4 inhibitor, Front. Immunol. 6 (2015) 276, https://doi.org/10.3389/fimmu.2015.00276.
[49] S. Hatse, K. Princen, G. Bridger, E. De Clercq, D. Schols, Chemokine receptor inhibition by AMD3100 is strictly confined to CXCR4, FEBS Lett. 527 (2002), https://doi.org/10.1016/S0014-5793(02)03143-5.
[50] M.V. Céspedes, U. Unzueta, P. Álamo, A. Gallardo, R. Sala, I. Casanova, M. A. Pavón, M.A. Mangues, M. Trías, A. López-Pousa, A. Villaverde, E. Vázquez, R. Mangues, Cancer-specific uptake of a liganded protein nanocarrier targeting aggressive CXCR4^{+}colorectal cancer models, Nanomedicine 12 (2016), https://doi.org/10.1016/j.nano.2016.04.003.
[51] J.M. Tarr, P.J. Young, R. Morse, D.J. Shaw, R. Haigh, P.G. Petrov, S.J. Johnson, P. G. Winyard, P. Eggleton, A mechanism of release of calreticulin from cells during apoptosis, J. Mol. Biol. 401 (2010), https://doi.org/10.1016/j.jmb.2010.06.064.
[52] T. Panaretakis, O. Kepp, U. Brockmeier, A. Tesniere, A.C. Bjorklund, D. C. Chapman, M. Durchschlag, N. Joza, G. Pierron, P. Van Endert, J. Yuan, L. Zitvogel, F. Madeo, D.B. Williams, G. Kroemer, Mechanisms of pre-apoptotic calreticulin exposure in immunogenic cell death, EMBO J. 28 (2009), https://doi.org/10.1038/emboj.2009.1.
[53] R. Osman, P. Tacnet-Delorme, J.P. Kleman, A. Millet, P. Frachet, Calreticulin release at an early stage of death modulates the clearance by macrophages of apoptotic cells, Front. Immunol. 8 (2017), https://doi.org/10.3389/fimmu.2017.01034.
[54] L. Zitvogel, O. Kepp, L. Senovilla, L. Menger, N. Chaput, G. Kroemer, Immunogenic tumor cell death for optimal anticancer therapy: the calreticulin exposure pathway, Clin Cancer Res 16 (12) (2010) 3100–3104, https://doi.org/10.1158/1078-0432.CCR-09-2891.
[55] S.H. Huang, L.X. Zhao, C. Hong, C.C. Duo, B.N. Guo, L.J. Zhang, Z. Gong, S. D. Xiong, F.Y. Gong, X.M. Gao, Self-oligomerization is essential for enhanced immunological activities of soluble recombinant calreticulin, PLoS One 8 (2013), https://doi.org/10.1371/journal.pone.0064951.
[56] C.S. Jørgensen, L.R. Ryder, A. Steinø, P. Højrup, J. Hansen, N.H. Beyer, N.H. H. Heegaard, G. Houen, Dimerization and oligomerization of the chaperone calreticulin, Eur. J. Biochem. 270 (2003), https://doi.org/10.1046/j.1432-1033.2003.03808.x.
[57] M.C. He, J. Wang, J. Wu, F.Y. Gong, C. Hong, Y. Xia, L.J. Zhang, W.R. Bao, X. M. Gao, Immunological activity difference between native calreticulin monomers and oligomers, PLoS One 9 (2014), https://doi.org/10.1371/journal.pone.0105502.
[58] S.J. Gardai, K.A. McPhillips, S.C. Frasch, W.J. Janssen, A. Starefeldt, J.E. Murphy-Ullrich, D.L. Bratton, P.A. Oldenborg, M. Michalak, P.M. Henson, Cell-surface calreticulin initiates clearance of viable or apoptotic cells through trans-activation of LRP on the phagocyte, Cell 123 (2005) 321–334, https://doi.org/10.1016/J.CELL.2005.08.032.
[59] C.B. Calson, P. Mowery, R.M. Owen, E.C. Dykhuizen, L.L. Kiessling, Selective tumor cell targeting using low-affinity, multivalent interactions, ACS Chem. Biol. 2 (2007), https://doi.org/10.1021/cb6003788.
[60] C.M. Csizmar, J.R. Petersburg, T.J. Perry, L. Rozumalski, B.J. Hackel, C.R. Wagner, Multivalent ligand binding to cell membrane antigens: defining the interplay of affinity, valency, and expression density, J. Am. Chem. Soc. 141 (2019), https://doi.org/10.1021/jacs.8b09198.
[61] A.R. Mendelsohn, J.W. Larrick, Antiaging Vaccines Targeting Senescent Cells, Rejuvenation Res. 25 (2022), https://doi.org/10.1089/rej.2022.0008.
[62] Y.N. Ding, H.Y. Wang, H.Z. Chen, D.P. Liu, Targeting senescent cells for vascular aging and related diseases, J. Mol. Cell. Cardiol. 162 (2022), https://doi.org/10.1016/j.yjmcc.2021.08.009.
[63] M. Paez-Ribes, E. González-Gualda, G.J. Doherty, D. Muñoz-Espín, Targeting senescent cells in translational medicine, EMBO Mol. Med. 11 (2019), https://doi.org/10.15252/emmm.201810234.
[64] D. Muñoz-Espín, Nanocarriers targeting senescent cells, Transl. Med. Aging 3 (2019) 1–5, https://doi.org/10.1016/j.tma.2019.01.001.
[65] S. Song, T. Tchkonia, J. Jiang, J.L. Kirkland, Y. Sun, Targeting senescent cells for a healthier aging: challenges and opportunities, Adv. Sci. 7 (23) (2020) 2002611, https://doi.org/10.1002/advs.202002611.
[66] N.S. Gasek, G.A. Kuchel, J.L. Kirkland, M. Xu, Strategies for targeting senescent cells in human disease, Nat. Aging 1 (10) (2021) 870–879, https://doi.org/10.1038/s43587-021-00121-8.